arXiv:2602.21819v3 [cs.CV] 17 Aug 2026

SemVideo: Reconstructs What You Watch from Brain Activity via Hierarchical Semantic Guidance

Minghan Yang[1], **Lan Yang**[1*], **Ke Li**[1], **Honggang Zhang**[1], **Kaiyue Pang**[2], **Yizhe Song**[2],
[1]Beijing University of Posts and Telecommunications
[2] University of Surrey
{yangminghan, ylan, like1990, zhhg}@bupt.edu.cn
hatkpang@gmail.com, y.song@surrey.ac.uk

Abstract

*Reconstructing dynamic visual experiences from brain activity provides an avenue for exploring the neural mechanisms of visual perception. While progress in fMRI-based image reconstruction has been notable, extending this success to video reconstruction remains a challenge. Current fMRI-to-video reconstruction approaches encounter two major shortcomings: (i) inconsistent visual representations of salient objects across frames, leading to appearance mismatches; (ii) poor temporal coherence, resulting in motion misalignment or abrupt frame transitions. To address these limitations, we introduce **SemVideo**, a fMRI-to-video reconstruction framework guided by hierarchical semantic information. At the core of SemVideo is **SemMiner**, a hierarchical guidance module that constructs three levels of semantic cues from the video stimulus: static anchor descriptions, motion-oriented narratives, and holistic summaries. Leveraging this semantic guidance, SemVideo comprises three key components: a Semantic Alignment Decoder that aligns fMRI signals with CLIP-style embeddings derived from SemMiner, a Motion Adaptation Decoder that reconstructs dynamic motion patterns using a novel tripartite attention fusion architecture, and a Conditional Video Render that leverages hierarchical semantic guidance for video reconstruction. Experiments on the CC2017 and HCP datasets demonstrate that SemVideo achieves superior performance in semantic alignment and temporal consistency, setting a new state-of-the-art in fMRI-to-video reconstruction. The code is publicly available at https://github.com/yang-minghan/SemVideo.*

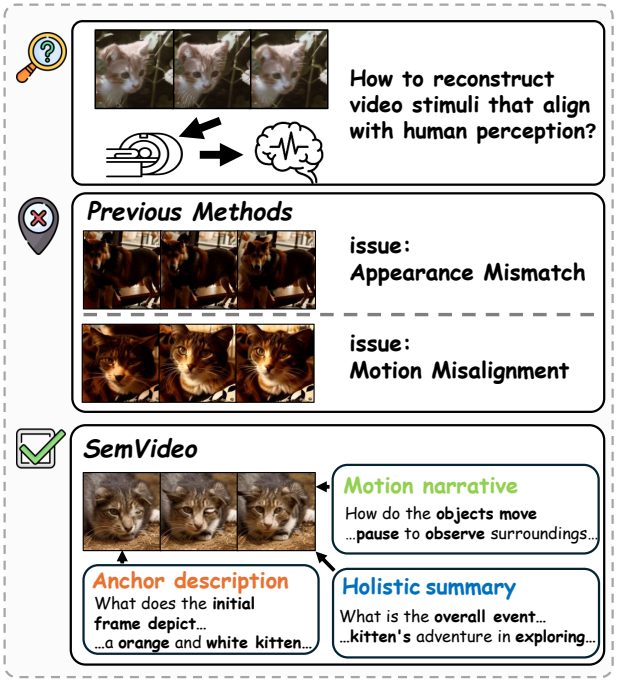

Figure 1. **Top:** While a subject watches an original video stimulus, their brain activity is recorded via fMRI. **Middle:** Reconstructed results from previous methods, which suffer from two issues: *Appearance Mismatch and Motion Misalignment*. **Bottom:** Reconstructed result from SemVideo, achieves both semantic consistency (reconstructing the "kitten") and motion coherence (matching dynamic actions like "crouching" and "turning") by leveraging hierarchical semantic descriptions as intermediate targets to guide the fMRI signal decoding process.

1. Introduction

Understanding the information encoded in brain activity remains one of the central challenges in cognitive neuroscience. Reconstructing external stimuli from brain signals — particularly using non-invasive methods such as functional Magnetic Resonance Imaging (fMRI) — is an important yet highly challenging task. Neural decoding typically encompasses three fundamental tasks[19]: classification, identification, and reconstruction. With the rapid

*Corresponding author

advancement of deep learning techniques, prior work has made remarkable progress in both the classification[30, 82] and identification[27, 31] of static visual stimuli from fMRI data. Notably, the release of the Natural Scenes Dataset (NSD)[1]—the largest publicly available fMRI-image paired dataset — has catalyzed significant breakthroughs in image reconstruction[8, 16, 62]. Moreover, the emergence of powerful text-to-image diffusion models has brought high-quality, high-resolution image reconstruction from fMRI signals within reach[9, 29, 42, 47, 53, 74, 75, 78, 79], transforming what was once considered an unattainable goal into a practical possibility.

However, reconstructing *dynamic visual stimuli* from fMRI signals remains a significant challenge due to the inherent limitations of fMRI, which relies on the slow hemodynamic response of BOLD signals. These signals integrate brain activity over several seconds, making it difficult to capture the rapid motion variations present in video stimuli. Consequently, fMRI-based video reconstruction becomes an even more complex and challenging task. Despite this, the development of video generation technology has greatly enhanced the feasibility of fMRI-based video reconstruction tasks[10, 13, 15, 43, 65]. However, two major issues remain unresolved in this task: (i) inconsistent visual representations of salient objects across frames, leading to appearance mismatches, and (ii) poor temporal coherence, resulting in motion misalignment or abrupt frame transitions.

In this work, inspired by neuroscience research indicating that the human brain perceives videos discretely[54, 60] due to phenomena such as persistence of vision[6, 7, 12, 49, 89] and delayed memory[33, 39, 70]. This makes it impractical for brain signals to process every video frame and every pixel; instead, only keyframes elicit significant responses from the brain's visual system. This suggests that focusing on key semantic perceptions, rather than exhaustive pixel-by-pixel analysis, aligns more closely with the efficiency and practicality of the human visual system.

To this end, we first propose *SemMiner*, a module built upon a multimodal large language model (MLLM [50–52, 68]), which decomposes the original video stimuli into fine-grained, multi-level textual descriptions including holistic summaries, static anchor descriptions, and motion-oriented narratives. This hierarchical supervision better simulates the way humans process and recall visual experiences, addressing the semantic under-specification problem in traditional pipelines. Guided by this hierarchical supervision, we then present *SemVideo*, a novel fMRI-to-video reconstruction framework guided by hierarchical semantic supervision and motion-aware latent decoding. Our framework is built upon three core components: (i) **Semantic Alignment Decoder.** To decode hierarchical semantic features from fMRI signals and adapt to the variable signal dimensions across different subjects, we propose the Semantic Alignment Decoder (SAD). This cross-subject multi-level semantic decoder consists of a subject-specific projector, a subject-shared mapper, and a Refineformer module, enabling precise semantic feature decoding from fMRI signals while minimizing noise. (ii) **Motion Adaptation Decoder.** To reconstruct coherent action sequences from brain signals, we designed the Motion Adaptation Decoder (MAD). The core of the MAD is a tripartite attention fusion architecture that synergistically integrates spatial self-attention, temporal self-attention, and semantic-guided cross-attention mechanisms. By explicitly injecting semantic priors into the attention computation, this module effectively aligns motion latents with both spatial structures and semantic actions, enhancing the fidelity and continuity of the reconstructed video dynamics. (iii) **Multi-Stage Semantic Fusion for Video Reconstruction**. We propose a multi-level, staged guidance strategy for conditional video generation. Instead of relying on a single semantic cue, we progressively condition the generation on three sources: static semantics (anchor descriptions), dynamic semantics (motion-oriented narratives), and holistic video-level semantics (holistic summaries). This structured conditioning ensures that the synthesized video aligns with both the static and temporal structure of the original perceptual input, yielding more coherent and realistic outputs.

Extensive experiments have demonstrated the superior performance and robustness of *SemVideo* on two widely-used public datasets, CC2017 [76] and HCP [44]. We evaluate our method against previous approaches across three dimensions: semantic-level, pixel-level, and spatiotemporal-level metrics, achieving SOTA performance on 8 out of 10 metrics. Additionally, we provide a neuroscience-based interpretation of the effectiveness of *SemVideo* using ROI-wise visualization techniques, which confirm that our hierarchical semantic descriptions activate corresponding brain regions and validate the model's effectiveness.

2. Related Work

2.1. Video Caption Generation

To introduce richer semantic guidance, a recent research [9, 18, 61, 62, 67, 74, 81] trend has shifted from unimodal visual feature alignment to dual-modal vision-text alignment. However, the effectiveness of this strategy is constrained by a significant bottleneck: the scarcity of high-quality, open-source video captioning models. Lacking dedicated video captioning tools, current research [13, 15, 43] often resort to applying Image Captioning models, such as GIT [73], BLIP [37, 38, 80] and SmallCap [56]), to discrete video frames. This method generates a series of short, static descriptions that fail to capture both the video's temporal dynamics and its fine-grained semantic details. Consequently, even when supervised by this textual modality, downstream

reconstruction models are unable to acquire comprehensive information about either motion or semantics. This dual deficiency is a primary cause of persistent issues with motion coherence and semantic accuracy in generated videos, representing a core challenge for the field.

2.2. Diffusion-based video generation

The feasibility of leveraging the fine-grained semantic guidance for the reconstruction task is critically dependent on the recent advancements in video generation. Building on the remarkable progress in image synthesis with diffusion models [23, 55, 58], the field has rapidly advanced to text-to-video (T2V) diffusion models [4, 26, 63]. These approaches, including 3D diffusion models [25] and methods such as AnimateDiff [20], excel at synthesizing temporally coherent motion strongly conditioned by textual descriptions. This ability to translate semantic intent into dynamic visual content positions them as the ideal generative backbone for fMRI-to-video decoding tasks.

2.3. fMRI-based Video Reconstruction

Early approaches [21, 35, 36, 46, 71, 76] to video reconstruction treated the task as a sequence of independent image reconstructions. These methods employed Generative Adversarial Networks (GANs [17]) or Autoencoders (AEs [34]) to synthesize frames from brain signals, with the primary goal of recovering low-level visual features. However, reconstructions from these models often lacked discernible semantic content. In contrast, recent studies have largely shifted toward generative frameworks centered on diffusion models [20, 24, 25]. One line of work, including Brain Netflix [13] and MinD-Video [10], utilizes masked-brain modeling (MBM) to map fMRI signals into a unified latent space that drives a video diffusion model. Another class of methods [15, 43, 65] focus on aligning fMRI signals with the deep features from pretrained models-such as CLIP embeddings or VAE encodings of video frames-to guide video reconstruction. Despite significant improvements in quality, these advanced methods still exhibit two primary limitations: insufficient motion coherence and semantic deviation. This gap highlights a pressing need for a more fine-grained semantic supervision mechanism to guide the video generation process.

3. Methodology

In this section, we present *SemMiner* and *SemVideo*, two key components of our proposed fMRI-to-video reconstruction method. *SemMiner* deconstructs a given video into fine-grained, multi-level textual descriptions, organizing them into three hierarchical semantic perspectives: first-frame appearance, motion cues, and overall temporal consistency. *SemVideo* is a decoding framework that transforms fMRI signals into semantic embeddings and motion latents, which are then used as conditional inputs for a text-to-video generation model to reconstruct the original video stimuli.

3.1. SemMiner

To provide precise and diverse semantic supervision for fMRI-to-video reconstruction, we introduce *SemMiner*, a hierarchical guidance module constructs three levels of semantic cues from the original video stimulus. Given a video stimulus V, these mined descriptions are structured into three complementary semantic perspectives. The **anchor description** C_{anchor} captures the static visual content of the first frame, serving as a semantic anchor to ensure basic alignment between the reconstructed and original videos. The **motion-oriented narratives** C_{motion} focus on fine-grained dynamic cues, particularly highlighting actions and dynamic transitions within the video. Finally, the **holistic summaries** C_{holi} encapsulate a global semantic summary of the entire video, integrating both static and motion information into a coherent narrative. These descriptions establish a comprehensive framework, providing multi-level semantic guidance for the reconstruction.

SemMiner is implemented as a two-stage semantic decomposition module. In the first stage, it generates a simple semantic summary C_{basic} of V using a MLLM Ψ [2, 84, 86], constrained to a maximum of 20 words, formulated as:

$$C_{\text{basic}} = \Psi(P_{\text{basic}}, V), \tag{1}$$

where P_{basic} denotes the initial instruction used for synthesizing the basic description. This short summary serves as a "rein", to prevent the subsequent generation of diverse captions from becoming overly unconstrained or drifting semantically—analogous to controlling a "runaway horse" [28, 32, 40, 88]. The imposed length limit ensures that C_{basic} captures only the most essential content, thereby reducing the risk of introducing strong priors that could dominate later stages.

In the second stage, *SemMiner* is steered by carefully crafted instructions P_L corresponding to specific semantic targets. Conditioned on the video V and the initial summary C_{basic}, the framework elicits the target-specific descriptions:

$$C_L = \Psi(P_L, C_{\text{basic}}, V), \quad L \in \{\text{anchor}, \text{motion}, \text{holi}\}, \tag{2}$$

where P_L denotes the instruction specifically designed for each semantic objective. The detailed instructions used in *SemMiner* can be found in Appendix A.1.

CC2017-SE. To advance the fMRI-to-video reconstruction field, we introduce CC2017-SE, a semantic extension of the CC2017 dataset. Building upon the original dataset, we apply *SemMiner* to generate three t semantic descriptions — C_{anchor}, C_{motion}, and C_{holi}. We also provide quantitative and qualitative analysis of synthesized captions in Appendix A.2. The extended dataset is available at https://huggingface.co/datasets/YanmHa/SemVideo.

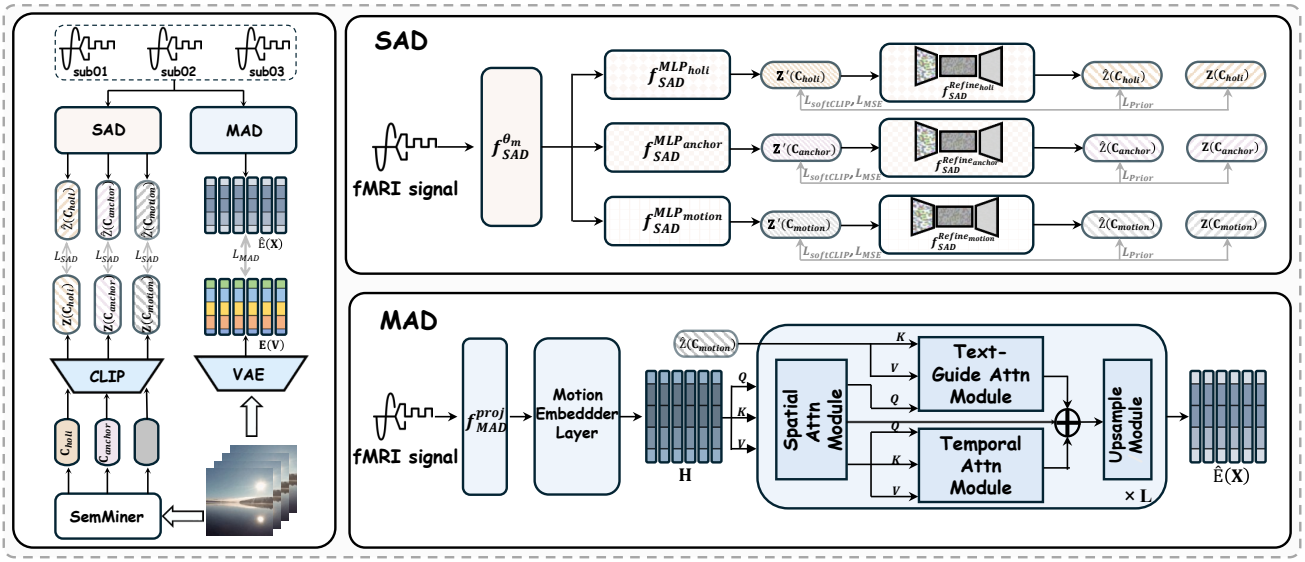

Figure 2. Overview of the *SemVideo* training pipeline. In the first stage, the Semantic Alignment Decoder is trained to map fMRI signals to three levels of semantic targets, denoted as $Z(C_L)$. In the second stage, the Motion Adaptation Decoder is trained to utilize the predicted motion semantics $\hat{Z}(C_{\text{motion}})$ to refine the latent embedding of each reconstructed frame.

3.2. SemVideo

SemVideo operates in three key stages, as illustrated in Figure.2 and Figure.3. First, the fMRI signals $X \in \mathbb{R}^{D_m}$ are decoded into semantic feature representations $\hat{Z}(C_L) \in \mathbb{R}^{77\times768}$, where D_m denotes the number of activated voxels for subject m, and $Z(\cdot)$ represents the target feature space. Second, it reconstructs a motion-guided latent representation of the video, denoted as $\hat{E}(X)$, guided by the decoded motion semantics $\hat{Z}(C_{\text{motion}})$. Finally, the decoded semantic and motion features are fused to generate the reconstructed video via Conditional Video Render Φ, formulated as:

$$\hat{V} = \Phi(\hat{Z}(C_{\text{anchor}}), \hat{Z}(C_{\text{holi}}), \hat{E}(X)). \tag{3}$$

Semantic Alignment Decoder (SAD) The objective of the Semantic Alignment Decoder (SAD) is to take the fMRI signal X as input and output the predicted semantic feature $\hat{Z}(C_L)$. Since the number of activated voxels varies across subjects, SAD first applies a subject-specific projection layer $f^{\theta_m}_{SAD}$ to project X into a unified latent space of dimension D_l, yielding $X' = f^{\theta_m}_{SAD}(X) \in \mathbb{R}^{D_l}$. Next, a subject-shared encoder f_{SAD} maps the normalized fMRI representation X' to the CLIP text feature space, resulting in $\hat{Z}(C_L) = f_{\text{SAD}}(X')$. The encoder f_{SAD} is composed of a four-layer multilayer perceptron (f^{MLP}_{SAD}) followed by a Refineformer (f^{Refine}_{SAD}), a causal transformer designed to maximize the extraction of meaningful neural activity while minimizing the influence of noise, thereby enhancing the alignment between fMRI signals and the target semantic space. The training of SAD is supervised by a combination of three training objectives:

$$\mathcal{L}_{\text{MSE}} = \left\| Z(C_L) - f^{MLP}_{\text{SAD}}(X') \right\|^2, \tag{4}$$

$$\mathcal{L}_{\text{SoftCLIP}} = -\sum_{j=1}^{B}\left[\frac{\exp\left(\frac{Z(C_L)\cdot Z(C_L^j)}{\tau}\right)}{\sum_{k=1}^{B}\exp\left(\frac{Z(C_L)\cdot Z(C_L^k)}{\tau}\right)} \times \log\left(\frac{\exp\left(\frac{f^{MLP}_{\text{SAD}}(X')\cdot Z(C_L^j)}{\tau}\right)}{\sum_{k=1}^{B}\exp\left(\frac{f^{MLP}_{\text{SAD}}(X')\cdot Z(C_L^k)}{\tau}\right)}\right)\right], \tag{5}$$

$$\mathcal{L}_{\text{refine}} = \mathbb{E}_{t\sim[1,T]}\left\| f^{Refine}_{\text{SAD}}\left(Z_L^t, t, f^{MLP}_{\text{SAD}}(X')\right) - Z(C_L)\right\|^2, \tag{6}$$

$$\mathcal{L}_{\text{SAD}} = \lambda_{\text{refine}}\,\mathcal{L}_{\text{refine}} + \lambda_{\text{SoftCLIP}}\,\mathcal{L}_{\text{SoftCLIP}} + \mathcal{L}_{\text{MSE}}, \tag{7}$$

where B denotes the batch size, j indexes the j-th sample in the batch, and τ is a temperature hyperparameter. T represents the total number of denoising timesteps, and Z_L^t is the perturbed semantic embedding of C_L at timestep t. λ_{refine} and $\lambda_{\text{SoftCLIP}}$ are weighting coefficients that balance the contributions of the corresponding loss components.

Motion Adaptation Decoder (MAD) To improve the fidelity of motion dynamics reconstructed from brain signals, we propose a semantically guided motion adaptation decoding strategy. Let the original video stimulus be denoted as $V = \{v_1, v_2, \cdots, v_n\}$, where n is the number of frames. We extract its motion latent representation using a pretrained VAE encoder $\mathbf{E}$, yielding $E(V) = \{e_1, e_2, \cdots, e_n\}$.

The objective of MAD is to take the fMRI signal X as input and generate a sequence of predicted motion la-

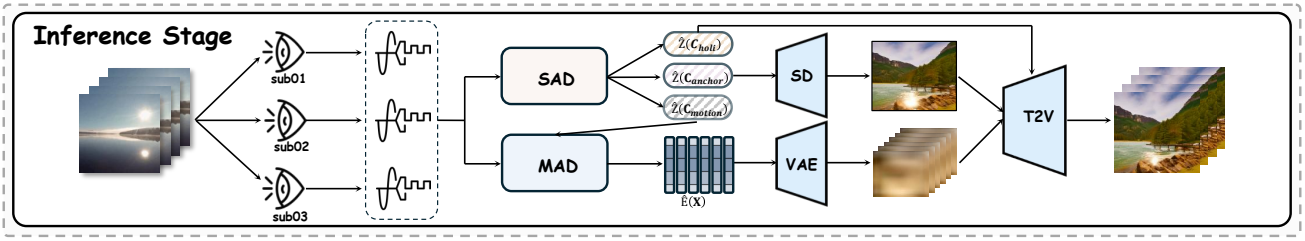

Figure 3. Overview of the *SemVideo* inference pipeline. fMRI signals are first decoded into $\hat{Z}(C_{\text{L}})$ by the SAD. $\hat{Z}(C_{\text{motion}})$ conditions the MAD to refine frame embeddings $\hat{E}(x)$, which are passed through a VAE decoder, generating a blurry video. $\hat{E}(x)$ and $\hat{Z}(C_{\text{anchor}})$ guide the SD model to generate anchor frame, combined with the blurry video and $\hat{Z}(C_{\text{holi}})$, is fed into a T2V model, yielding final reconstruction.

tents corresponding to the reconstructed video frames, denoted as $\hat{E}(X) = \{\hat{e}_1, \hat{e}_2, \cdots, \hat{e}_n\}$. To achieve this, MAD first projects the fMRI signal into the latent space using a subject-specific projection network f^{proj}_{MAD}, implemented as a multilayer perceptron [1]. This projection yields a latent tensor $g = f^{proj}_{\text{MAD}}(X) \in \mathbb{R}^{n \times D_{\text{emb}}}$, where D_{emb} denotes the embedding dimension. Next, the tensor g is processed by a Motion Embedder Layer to produce a sequence of embeddings $S = \{s_1, s_2, \cdots, s_n\} \in \mathbb{R}^{n \times c \times h \times w}$, where $c \times h \times w$ is the dimension of the embedding latent space. This embedding sequence serves as the initial input to the subsequent attention-based decoding module. MAD conducts a hierarchical fusion attention mechanism:

(i) To capture intra-frame structure, we apply *spatial attention* to each s_i. The latent tensor is reshaped and attended via scaled dot-product attention:

$$\hat{S} = \text{Reshape}(S) \in \mathbb{R}^{(n \cdot h \cdot w) \times c}, \tag{8}$$

$$E_{\text{spat}} = \text{Softmax}\left(\frac{Q_{\text{spat}} K_{\text{spat}}^{\top}}{\sqrt{d}}\right) V_{\text{spat}}, \tag{9}$$

where $Q_{\text{spat}} = \hat{S}W_{Q_{\text{spat}}}, K_{\text{spat}} = \hat{S}W_{K_{\text{spat}}}, V_{\text{spat}} = \hat{S}W_{V_{\text{spat}}}$.

(ii) To model inter-frame dependencies, we apply *temporal attention* across the temporal axis. We first flatten each spatially attended frame into a temporal sequence:

$$\tilde{S} = \text{Reshape}(E_{\text{spat}}) \in \mathbb{R}^{(c \cdot h \cdot w) \times n}, \tag{10}$$

The attention computation follows the same formulation as in the spatial attention and is omitted here for brevity.

(iii) We further incorporate *semantic guided cross-attention*. Let $\hat{Z}(C_{\text{motion}})$ be the predicted motion descriptions from the video, as formulated by:

$$E_{\text{cross}} = \text{Softmax}\left(\frac{Q_{\text{cross}} K_{\text{cross}}^{\top}}{\sqrt{d}}\right) V_{\text{cross}}, \tag{11}$$

where $Q_{\text{cross}} = \tilde{S}W_{Q_{\text{cross}}}, K_{\text{cross}} = \hat{Z}(C_{\text{motion}})W_{K_{\text{cross}}}$ and $V_{\text{cross}} = \hat{Z}(C_{\text{motion}})W_{V_{\text{cross}}}$. Finally, the output of MAD can be represented as:

$$\hat{e}_i = \lambda_{\text{spat}}\, e_i^{\text{spat}} + \lambda_{\text{temp}}\, e_i^{\text{temp}} + e_i^{\text{cross}}, \tag{12}$$

[1] The architecture of f^{proj}_{MAD} is detailed in Appendix C.1

where λ_{spat} and λ_{temp} are weights for e_{spat} and e_{temp}, respectively. The training objectives of MAD are formulated by:

$$\begin{aligned}\mathcal{L}_{MAD} =& \frac{1}{n}\sum_{i=1}^{n}|\hat{e}_i - e_i| \\ &- \frac{1}{2n}\sum_{j=1}^{n}\log\frac{\exp\left(\text{sim}(\hat{e}_j, e_j)/\tau\right)}{\sum_{k=1}^{n}\exp\left(\text{sim}(\hat{e}_j, e_k)/\tau\right)} \\ &- \frac{1}{2n}\sum_{j=1}^{n}\log\frac{\exp\left(\text{sim}(e_j, \hat{e}_j)/\tau\right)}{\sum_{k=1}^{n}\exp\left(\text{sim}(e_j, \hat{e}_k)/\tau\right)}\end{aligned} \tag{13}$$

where $\text{sim}(\cdot,\cdot)$ is cosine similarity.

Conditional Video Render (CVR) To fully leverage the information decoded from fMRI signals, we design CVR — a sequential inference framework that reconstructs the video by progressively integrating the fMRI-derived cues at each stage of the generation process. First, the decoded motion latents $\hat{E}(X) = \{\hat{e}_1, \hat{e}_2, \ldots, \hat{e}_n\}$ are passed through the pretrained VAE decoder $\mathbf{D}$ to produce a sequence of motion frames $\{I_i^{\text{motion}}\}_{i=1}^{n}$. Next, the decoded anchor feature $\hat{Z}(C_{\text{anchor}})$ is combined with the first motion frame I_1^{motion} and fed into a text-to-image (T2I) model, yielding the initial reconstructed frame $\hat{v}_1$. Finally, a pretrained text-to-video (T2V) generator is steered jointly by three sources: (i) the holistic semantic guidance $\hat{Z}(C_{\text{holi}})$, (ii) the anchor frame $\hat{v}_1$, and (iii) the motion-frame sequence $\{I_i^{\text{motion}}\}_{i=1}^{n}$. This combination encourages both temporal smoothness and semantic fidelity, enabling CVR to synthesize a coherent video that closely matches the original visual stimulus inferred from the fMRI signals.

4. Experiments

Datasets and Pre-processing: We evaluate our method on two publicly available fMRI-video datasets: CC2017 [76] and a subset of the HCP 7T dataset [44]. **CC2017** contains fMRI recordings from three subjects (3T MRI) while watching 23 high-definition natural movie clips (8 minutes each, 30 FPS). To improve signal-to-noise ratio (SNR), training clips are repeated twice and test clips ten times; the fMRI responses are averaged accordingly. After aligning

Method	Semantic-Level					Pixel-Level			ST-Level	
	2-way-I↑	2-way-V↑	50-way-I↑	50-way-V↑	VIFI-score↑	SSIM↑	PSNR↑	Hue-pcc↑	CLIP↑	EPE ↓
Nishimoto [46](Current Biology'11)	0.742	–	–	–	–	0.119	8.383	0.737	–	–
Wen [76](Cerebral Cortex'17)	0.771	0.070	–	0.166	–	0.130	8.301	0.637	–	–
Kupershmidt [35](arXiv'22)	0.769	0.768	0.179	–	0.591	0.108	11.030	0.583	0.399	6.344
f-CVGAN [71](Cerebral Cortex'22)	0.777	0.721	–	–	0.592	0.108	**11.430**	0.583	0.399	6.344
Mind-video [10](NeurIPS'23)	0.797	0.848	0.174	0.197	0.593	0.177	8.868	0.768	0.409	6.125
NeuroClips [15](NeurIPS'25)	0.806	0.834	0.203	0.220	0.602	**0.390**	9.211	0.812	0.513	4.833
Mind-Animator [43](ICLR'25)	0.805	0.830	0.192	0.186	**0.608**	0.321	9.220	0.786	0.425	5.422
NEURONS [72](ICCV'25)	0.815	0.853	0.213	0.246	0.597	0.285	9.526	0.830	0.482	4.827
Ours	**0.838**	**0.865**	**0.225**	**0.264**	**0.608**	0.321	9.448	**0.849**	**0.526**	**4.788**

Table 1. Quantitative comparison of reconstruction results on the CC2017 dataset. All metrics are averaged across all samples and three subjects, with the best results highlighted in bold and the second-best results underlined. 100 sample sets were constructed using the bootstrap method for hypothesis testing. Colors reflect statistical significance compared to our model. $p < 0.0001$(blue); $p < 0.01$(pink); $p < 0.05$(yellow); $p > 0.05$(green)

.

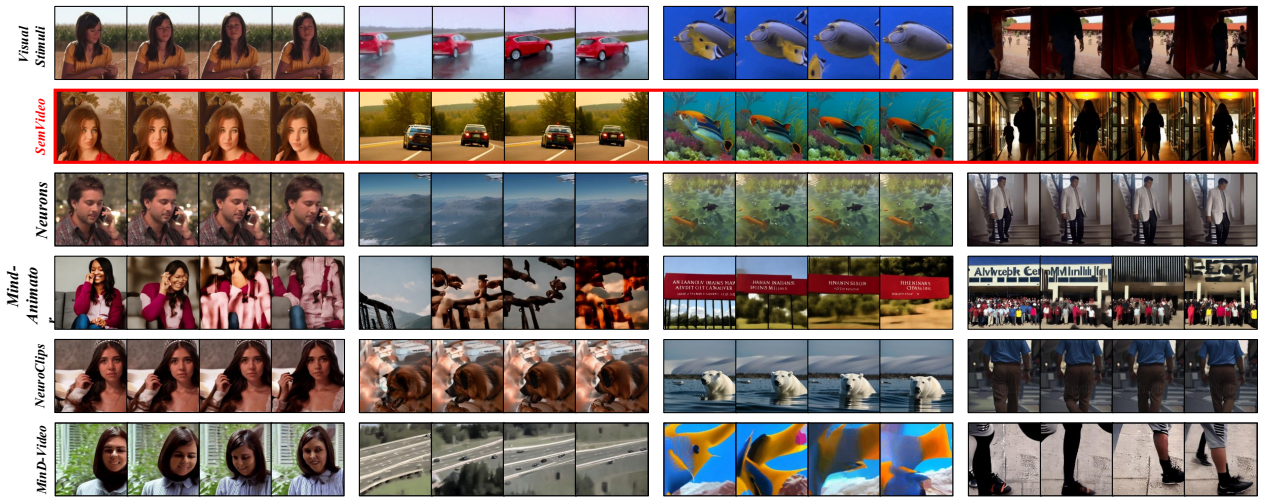

Figure 4. Qualitative comparison of reconstruction results on the CC2017 dataset between previous methods and our proposed *SemVideo*. Reconstructions generated by *SemVideo*are highlighted with red boxes.

Method	Semantic		Pixel		ST-Level	
	2-way-I↑	2-way-V↑	PSNR↑	Hue-pcc↑	CLIP ↑	EPE ↓
Nishimoto	0.658	–	**11.316**	0.645	–	–
Wen	0.702	–	10.197	0.727	–	–
Mind-video	0.779	0.769	9.275	0.793	0.499	9.29
Mind-Animator	0.786	0.778	11.233	0.829	0.511	7.08
Ours	**0.815**	**0.796**	9.336	**0.858**	**0.523**	**4.05**

Table 2. Quantitative comparison on the HCP dataset.

video frames with the fMRI temporal resolution (TR = 2s), we obtain 8,640 training samples and 1,200 test samples. Visually responsive voxels are selected by computing the temporal correlation between repeated presentations, applying Fisher's z-transform, and conducting a one-sample t-test (Bonferroni corrected, $p < 0.05$). This yields 13,447; 14,828; and 9,114 voxels for the three subjects, respectively. A 4-second BOLD lag is applied to compensate for the hemodynamic response delay. **HCP 7T**: We use a subset of the HCP 7T dataset, selecting three subjects (IDs: 100610, 102816, 104416) following prior work. The data undergoes HCP's preprocessing pipeline, including motion/distortion correction, high-pass filtering, ICA denoising, and MNI registration. We extract 5,820 voxels from [14]. We partition clips into training and test sets with a 9:1 split. A 4-second hemodynamic lag is similarly applied.

Evaluation Metrics : We follow previous works that introduce the evaluation metrics at three complementary levels: **Semantic-Level**: (i) *N-way top-1 retrieval* in four settings—2-way/50-way, frame-level [11]]/video-level [69]. (ii) *VIFI* [57]: cosine similarity of VIFICLIP features between ground-truth and reconstructions. **Pixel-Level**: SSIM, PSNR, and Hue-PCC [66] quantify low-level fidelity. **Spatiotemporal-Level (ST-Level)**: (i) *CLIP-PCC*:

Method	Semantic-Level					Pixel-Level			ST-Level	
	2-way-I↑	2-way-V↑	50-way-I↑	50-way-V↑	VIFI-score↑	SSIM↑	PSNR↑	Hue-pcc↑	CLIP ↑	EPE ↓
Ours (full)	**0.826**	**0.860**	**0.211**	**0.239**	**0.590**	0.330	**9.626**	**0.841**	**0.502**	**4.768**
w/o C_{anchor}	0.786	0.808	0.158	0.147	0.534	**0.361**	9.454	0.835	0.488	4.796
w/o C_{holi}	0.819	0.849	0.205	0.221	0.584	0.299	9.492	0.834	0.490	4.859
w/o C_{motion}	0.818	0.846	0.207	0.216	0.583	0.285	9.353	0.741	0.481	4.930

Table 3. Ablation study evaluating the impact of removing different semantic descriptions—C_{anchor}, C_{holi}, and C_{motion}—from the decoding targets of the Semantic Alignment Decoder (SAD). All results are reported from subj01 of the CC2017 dataset.

average cosine similarity of CLIP embeddings of adjacent frames; set to 0 when VIFI < 0.6 to avoid spurious inflation. (ii) *EPE* [3]: quantifies motion fidelity by calculating the average Euclidean distance between predicted and ground-truth optical flow vectors at each pixel.

Implementation: The training strategy of the experiment involves pre-training across all subjects, followed by fine-tuning on a single subject. Consistent with prior research [15], we adopt AnimateDiff for T2V task. All models are trained for 100 epochs with AdamW. Loss weights are $\lambda_{\text{SoftCLIP}}$=0.1 and λ_{refine}=0.5. Please refer to Appendix C.1 for more implementation details.

4.1. Main Results

We report the quantitative performance of our method on the CC2017 dataset in Table.1 and qualitative comparisons in Figure.4. *SemVideo* achieves remarkable and comprehensive performance across all evaluation levels.

Superior Semantic Accuracy and Fidelity. Our model outperforms NeuroClips [15] and Neurons [72], achieving a 2-way-V score of 0.865 and a 50-way-V score of 0.264, demonstrating superior semantic consistency and discriminability. On the VIFI-score, which reflects overall semantic-video alignment, *SemVideo* ties with MindAnimator[43] at 0.608, indicating strong semantic fidelity. This quantitative superiority is also reflected visually in Figure.4 where the reconstructions of *SemVideo* are more aligned with the ground truth video stimuli, accurately capturing central objects like "fish" and "cars".

Competitive Low-Level Reconstruction Quality. For pixel-level reconstruction quality, our model achieves the highest hue-pcc (0.849) and reaches a competitive SSIM of 0.321 and PSNR of 9.448, closely trailing the SoTA method. This high fidelity is also evident visually, as it effectively recovers key low-level features such as lighting and shadow contrasts (e.g., rightmost column in Figure.4).

Enhanced Spatial-Temporal Coherence. Our model achieves the highest CLIP similarity (0.526), and the lowest EPE (4.788), highlighting better preservation of spatial-temporal coherence and alignment with high-level perceptual features. Most notably, this is demonstrated by *SemVideo*'s ability to excel at modeling temporal dynamics, successfully reconstructing coherent motion patterns—such as "a person turning their head" (Figure.4, first column)—which remain challenging for previous methods. These results underscore *SemVideo*'s strength in preserving both spatial detail and temporal consistency in fMRI-to-video reconstruction.

Strong Generalization Ability. To assess generalization, we further evaluate on the HCP dataset. As shown in Table.2, *SemVideo* maintains strong performance, demonstrating its robustness across subjects and datasets.

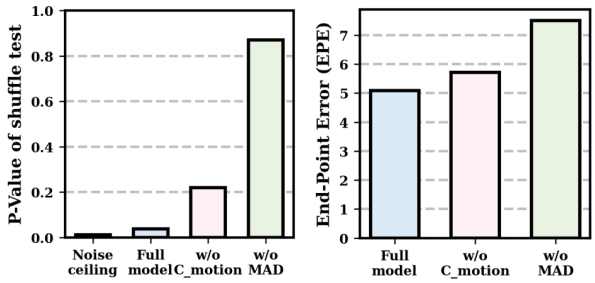

Figure 5. The figure presents two sets of results from subj01 of the CC2017 dataset. On the left, the results of a shuffle test are shown. On the right, the results of an ablation study are displayed, evaluating the impact of the C_{motion} and MAD guidance components.

4.2. Validating the Source of Motion Improvement.

Following the work of [43], we reconstruct video clips using Tune-a-video [77] which lacks motion priors and conduct shuffle tests to further validate the contributions of both the MAD and the motion-oriented narratives C_{motion} to motion improvement. Specifically, for each 12-frame reconstructed video, we randomly shuffle the order of the frames 100 times and compute the EPE on both the original and shuffled frames. We estimate the P-value using the following formula: $P = \sum_{i=1}^{100} \delta_i / 100$, where $\delta_i = 1$ if the i^{th} shuffle outperforms the reconstruction result in the original order based on the metrics, and $\delta_i = 0$ otherwise. A lower P-value signifies a closer alignment between the sequential order of the reconstructed video and the ground truth. It can be observed that the P-value for our full model is significantly low, confirming that its predicted inter-frame order robustly matches the ground truth, but rises substantially

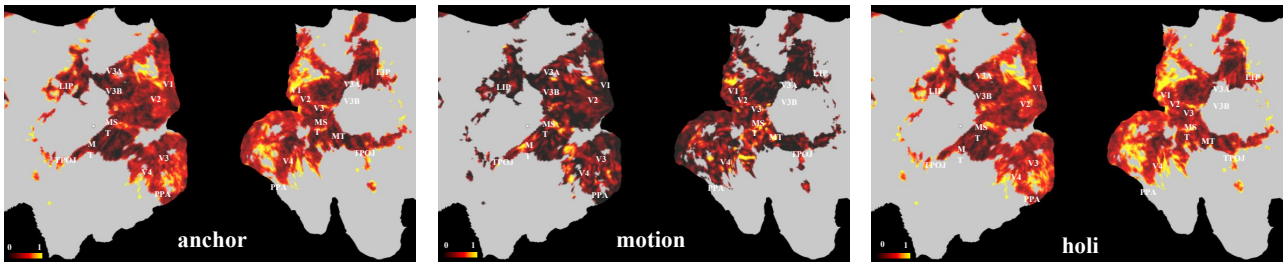

Figure 6. Importance visualization of different ROIs of subject 1 on CC2017, based on the fitted weights from the first layer of the SAD. Weights from each module are averaged and normalized to the $[0, 1]$ range for comparison. Please refer to Appendix D for more subjects' importance visualization.

when C_{motion} is removed and spikes to 0.84 when the entire MAD is ablated, as illustrated in Figure.5 left. This indicates that we have indeed decoded motion information from MAD and fMRI-derived C_{motion}. This conclusion is reinforced by a comparison of the EPE score, as shown in Figure.5 right. The EPE increase when removing C_{motion} and the spike when ablating the MAD confirm the crucial role of motion semantic guidance and that the MAD, not T2V priors, is the source of decoded motion improvement.

4.3. Ablation Study

In this section, we conduct a detailed ablation study to evaluate the individual contributions of the C_{anchor}, C_{holi}, and C_{motion} components to our *SemVideo*. The quantitative results, presented in Table.3, unequivocally demonstrate that the removal of any single component leads to a performance degradation across nearly all metrics, affirming their indispensability. Specifically, the exclusion of C_{motion} causes the most precipitous decline in pixel-level and ST-level metrics. The absence of C_{anchor}, in contrast, significantly impairs semantic-level fidelity. The C_{holi} proves integral for overall performance, as its removal adversely affects all metrics, underscoring its global guidance under video reconstruction. Crucially, and in contrast to prior works employing conventional latent decoders, the removal of C_{motion} also results in a notable drop in semantic metrics. This key finding substantiates the efficacy of our multi-level semantic guidance mechanism. It demonstrates that our motion latent space is not only responsible for ensuring pixel-level consistency and temporal smoothness but is also endowed with semantic understanding, thereby guaranteeing the coherence of the synthesized actions.

4.4. Neuroscience Interpretability

To investigate the neural interpretability of our model, we generated voxel-wise importance maps over the cerebral cortex. The results, presented in Figure.6, shed light on the neural substrates underlying each core component. The anchor component (Figure.6, left) predominantly draws from a hierarchy of visual regions, with a notable emphasis on higher-level visual cortices, confirming its role in encoding abstract scene structure. The motion component (Figure.6, middle) aligns well with established motion-processing regions, including MT, MST, and TPOJ [5]. Interestingly, it also shows strong activations in V1, supporting the existence of parallel, non-hierarchical pathways—where V1 may directly convey motion signals to MT [45]—in contrast to the traditional view of a strictly feedforward dorsal stream [83]. Lastly, the holistic component (Figure.6, right) exhibits a distributed pattern of importance across both visual and motion-related areas. This balanced integration highlights its function as a global information aggregator, responsible for synthesizing perceptual and temporal features to support coherent reconstruction. This hierarchical semantic mapping enables *SemVideo* to generate more perceptually faithful reconstructions and similar activation distributions across subjects demonstrate stable feature capture for both static semantics and dynamic behaviors.

5. Conclusion

Reconstructing dynamic visual stimuli from brain activity remains a challenge in cognitive neuroscience. In this work, we propose *SemVideo*, an innovative fMRI-to-video reconstruction framework featuring a novel semantic alignment decoder, a motion adaptation decoder and a conditional video render. By leveraging multi-level semantic cues, *SemVideo* effectively addresses the challenges of both semantic sparsity and temporal coherence in video reconstruction. Our experimental evaluation demonstrates the superior performance of *SemVideo* on two public datasets, surpassing existing methods across multiple metrics, including semantic, pixel, and spatiotemporal levels. Furthermore, our use of ROI-wise visualization techniques provides valuable neuroscience-driven insights into the effectiveness of the proposed method. We believe *SemVideo* will set a new SOTA in fMRI-to-video decoding and lay the foundation for future brain-based video reconstruction.

Acknowledgement

This work was supported in part by the Beijing Natural Science Foundation under Grant QY25342; in part by the National Natural Science Foundation of China under Grant 62502045; in part by the Postdoctoral Fellowship Program of CPSF under Grant GZC20251088.

References

[1] Emily J Allen, Ghislain St-Yves, Yihan Wu, Jesse L Breedlove, Jacob S Prince, Logan T Dowdle, Matthias Nau, Brad Caron, Franco Pestilli, Ian Charest, et al. A massive 7t fmri dataset to bridge cognitive neuroscience and artificial intelligence. *Nature Neuroscience*, 25:116–126, 2022. 2

[2] Shuai Bai, Keqin Chen, Xuejing Liu, Jialin Wang, Wenbin Ge, Sibo Song, Kai Dang, Peng Wang, Shijie Wang, Jun Tang, Humen Zhong, Yuanzhi Zhu, Mingkun Yang, Zhaohai Li, Jianqiang Wan, Pengfei Wang, Wei Ding, Zheren Fu, Yiheng Xu, Jiabo Ye, Xi Zhang, Tianbao Xie, Zesen Cheng, Hang Zhang, Zhibo Yang, Haiyang Xu, and Junyang Lin. Qwen2.5-vl technical report. *arXiv preprint arXiv:2502.13923*, 2025. 3, 13

[3] John L. Barron, David J. Fleet, and Steven S. Beauchemin. Performance of optical flow techniques. *International Journal of Computer Vision*, 12:43–77, 1994. 7, 16

[4] Andreas Blattmann, Robin Rombach, Huan Ling, Tim Dockhorn, Seung Wook Kim, Sanja Fidler, and Karsten Kreis. Align your latents: High-resolution video synthesis with latent diffusion models. In *CVPR*, 2023. 3

[5] Richard T. Born and David C. Bradley. Structure and function of visual area mt. *Annual Review of Neuroscience*, 28: 157–189, 2005. 8

[6] Andreas Brøgger and Karen Newman. Persistence of vision: the interplay of vision. In *Vision, Memory and Media*, page 13. 2010. 2

[7] Guangyi Chen, Yifan Shen, Zhenhao Chen, Xiangchen Song, Yuewen Sun, Weiran Yao, Xiao Liu, and Kun Zhang. Caring: Learning temporal causal representation under non-invertible generation process. *arXiv preprint arXiv:2401.14535*, 2024. 2

[8] Jiaxuan Chen, Yu Qi, Yueming Wang, and Gang Pan. Mind artist: Creating artistic snapshots with human thought. In *CVPR*, 2024. 2

[9] Zijiao Chen, Jiaxin Qing, Tiange Xiang, Wan Lin Yue, and Juan Helen Zhou. Seeing beyond the brain: Conditional diffusion model with sparse masked modeling for vision decoding. In *CVPR*, 2023. 2

[10] Zijiao Chen, Jiaxin Qing, and Juan Helen Zhou. Cinematic mindscapes: high-quality video reconstruction from brain activity. In *NeurIPS*, 2023. 2, 3, 6

[11] Alexey Dosovitskiy, Lucas Beyer, Alexander Kolesnikov, Dirk Weissenborn, Xiaohua Zhai, Thomas Unterthiner, Mostafa Dehghani, Matthias Minderer, Georg Heigold, Sylvain Gelly, Jakob Uszkoreit, and Neil Houlsby. An image is worth 16x16 words: Transformers for image recognition at scale. In *CVPR*, 2021. 6, 15

[12] Ervin S Ferry. Persistence of vision. *American Journal of Science*, 3(261):192–207, 1892. 2

[13] Camilo Fosco, Benjamin Lahner, Bowen Pan, Alex Andonian, Emilie Josephs, Alex Lascelles, and Aude Oliva. Brain netflix: Scaling data to reconstruct videos from brain signals. In *ECCV*, 2024. 2, 3

[14] Matthew F Glasser, Timothy S Coalson, Emma C Robinson, Carl D Hacker, John Harwell, Essa Yacoub, Kamil Ugurbil, Jesper Andersson, Christian F Beckmann, Mark Jenkinson, et al. A multi-modal parcellation of human cerebral cortex. *Nature*, 536(7615):171–178, 2016. 6

[15] Zixuan Gong, Guangyin Bao, Qi Zhang, Zhongwei Wan, Duoqian Miao, Shoujin Wang, Lei Zhu, Changwei Wang, Rongtao Xu, Liang Hu, et al. Neuroclips: Towards high-fidelity and smooth fmri-to-video reconstruction. In *NeurIPS*, 2024. 2, 3, 6, 7, 13

[16] Zixuan Gong, Qi Zhang, Guangyin Bao, Lei Zhu, Rongtao Xu, Ke Liu, Liang Hu, and Duoqian Miao. Mindtuner: Cross-subject visual decoding with visual fingerprint and semantic correction. In *AAAI*, 2025. 2

[17] Ian J. Goodfellow, Jean Pouget-Abadie, Mehdi Mirza, Bing Xu, David Warde-Farley, Sherjil Ozair, Aaron Courville, and Yoshua Bengio. Generative adversarial nets. In *NeurIPS*, 2014. 3

[18] Zijin Gu, Keith Jamison, Amy Kuceyeski, and Mert Sabuncu. Decoding natural image stimuli from fmri data with a surface-based convolutional network. In *MIDL*, 2024. 2

[19] Weiyu Guo, Guoying Sun, JianXiang He, Tong Shao, Shaoguang Wang, Ziyang Chen, Meisheng Hong, Ying Sun, and Hui Xiong. A survey of fmri to image reconstruction. *arXiv preprint arXiv:2502.16861*, 2025. 1

[20] Yuwei Guo, Ceyuan Yang, Anyi Rao, Zhengyang Liang, Yaohui Wang, Yu Qiao, Maneesh Agrawala, Dahua Lin, and Bo Dai. Animatediff: Animate your personalized text-to-image diffusion models without specific tuning. In *ICLR*, 2024. 3

[21] K. Han, H. Wen, J. Shi, K. H. Lu, Y. Zhang, D. Fu, and Z. Liu. Variational autoencoder: An unsupervised model for encoding and decoding fmri activity in visual cortex. *NeuroImage*, 198:125–136, 2019. 3

[22] Jack Hessel, Ari Holtzman, Maxwell Forbes, Ronan Le Bras, and Yejin Choi. Clipscore: A reference-free evaluation metric for image captioning. In *EMNLP*, 2021. 13

[23] Jonathan Ho, Ajay Jain, and Pieter Abbeel. Denoising diffusion probabilistic models. In *NeuIPS*, 2020. 3

[24] Jonathan Ho, William Chan, Chitwan Saharia, Jay Whang, Ruiqi Gao, Alexey Gritsenko, Diederik P. Kingma, Ben Poole, Mohammad Norouzi, David J. Fleet, and Tim Salimans. Imagen video: High definition video generation with diffusion models. *arXiv preprint arXiv:2210.02303*, 2022. 3

[25] Jonathan Ho, Tim Salimans, Alexey Gritsenko, William Chan, Mohammad Norouzi, and David J. Fleet. Video diffusion models. In *NeurIPS*, 2022. 3

[26] Wenyi Hong, Ming Ding, Wendi Zheng, Xinghan Liu, and Jie Tang. Cogvideo: Large-scale pretraining for text-to-video generation via transformers. In *ICLR*, 2023. 3

[27] Tomoyasu Horikawa and Yukiyasu Kamitani. Generic decoding of seen and imagined objects using hierarchical visual features. *Nature Communications*, 8:15037, 2015. 2

[28] Lei Huang, Weijiang Yu, Weitao Ma, Weihong Zhong, Zhangyin Feng, Haotian Wang, Qianglong Chen, Weihua Peng, Xiaocheng Feng, Bing Qin, and Ting Liu. A survey on hallucination in large language models: Principles, taxonomy, challenges, and open questions. *ACM Transactions on Information Systems*, 43(2), 2025. 3, 13

[29] Jingyang Huo, Yikai Wang, Xuelin Qian, Yun Wang, Chong Li, Jianfeng Feng, and Yanwei Fu. Neuropictor: Refining fmri-to-image reconstruction via multi-individual pretraining and multi-level modulation. In *ECCV*, 2024. 2

[30] Yukiyasu Kamitani and Frank Tong. Decoding the visual and subjective contents of the human brain. nature neurosci. *Nature Neuroscience*, 8:679–85, 2005. 2

[31] Kendrick N Kay, Thomas Naselaris, Ryan J Prenger, and Jack L Gallant. Identifying natural images from human brain activity. *Nature*, 452:352–355, 2008. 2

[32] Tushar Khot, Harsh Trivedi, Matthew Finlayson, Yao Fu, Kyle Richardson, Peter Clark, and Ashish Sabharwal. Decomposed prompting: A modular approach for solving complex tasks. In *ICLR*, 2023. 3, 13

[33] Seong-Gi Kim and Seiji Ogawa. Biophysical and physiological origins of blood oxygenation level-dependent fmri signals. *Journal of Cerebral Blood Flow & Metabolism*, 32(7): 1188–1206, 2012. 2

[34] Diederik P Kingma and Max Welling. Auto-encoding variational bayes. In *ICLR*, 2014. 3

[35] Ganit Kupershmidt, Roman Beliy, Guy Gaziv, and Michal Irani. A penny for your (visual) thoughts: Self-supervised reconstruction of natural movies from brain activity. *arXiv preprint arXiv:2206.03544*, 2022. 3, 6

[36] L. Le, L. Ambrogioni, K. Seeliger, Y. Güçlütürk, M. van Gerven, and U. Güçlü. Brain2pix: Fully convolutional naturalistic video frame reconstruction from brain activity. *Frontiers in Neuroscience*, 16:940972, 2022. 3

[37] Junnan Li, Dongxu Li, Caiming Xiong, and Steven Hoi. BLIP: Bootstrapping language-image pre-training for unified vision-language understanding and generation. In *ICML*, 2022. 2

[38] Junnan Li, Dongxu Li, Silvio Savarese, and Steven Hoi. Blip-2: bootstrapping language-image pre-training with frozen image encoders and large language models. In *ICML*, 2023. 2

[39] Nikos K Logothetis. The neural basis of the blood–oxygen–level–dependent functional magnetic resonance imaging signal. *Philosophical Transactions of the Royal Society of London. Series B: Biological Sciences*, 357(1424):1003–1037, 2002. 2

[40] Do Xuan Long, Duong Ngoc Yen, Anh Tuan Luu, Kenji Kawaguchi, Min-Yen Kan, and Nancy F. Chen. Multi-expert prompting improves reliability, safety, and usefulness of large language models. In *EMNLP*, 2024. 3, 13

[41] Ilya Loshchilov and Frank Hutter. Decoupled weight decay regularization. *arXiv preprint arXiv:1711.05101*, 2019. 16

[42] Bizhuo Lu, Changde Du, Qiongyi Zhou, Dianpeng Wang, and Huiguang He. Minddiffuser: Controlled image reconstruction from human brain activity with semantic and structural diffusion. In *ACM MM*, 2023. 2

[43] Yizhuo Lu, Changde Du, Chong Wang, Xuanliu Zhu, Liuyun Jiang, and Huiguang He. Animate your thoughts: Decoupled reconstruction of dynamic natural vision from slow brain activity. In *ICLR*, 2025. 2, 3, 6, 7, 13

[44] Daniel S Marcus, John Harwell, Timothy Olsen, Michael Hodge, Matthew F Glasser, Fred Prior, Mark Jenkinson, Timothy Laumann, Sandra W Curtiss, and David C Van Essen. Informatics and data mining tools and strategies for the human connectome project. *Frontiers in Neuroinformatics*, 5:4, 2011. 2, 5, 17

[45] Jonathan J. Nassi and Edward M. Callaway. Parallel processing strategies of the primate visual system. *Nature Reviews Neuroscience*, 10(5):360–372, 2009. 8

[46] S. Nishimoto, A. T. Vu, T. Naselaris, Y. Benjamini, B. Yu, and J. L. Gallant. Reconstructing visual experiences from brain activity evoked by natural movies. *Current Biology*, 21 (19):1641–1646, 2011. 3, 6

[47] Furkan Ozcelik and Rufin VanRullen. Brain-diffuser: Natural scene reconstruction from fmri signals using generative latent diffusion. *Scientific Reports*, 13, 2023. 2

[48] Kishore Papineni, Salim Roukos, Todd Ward, and Wei-Jing Zhu. Bleu: a method for automatic evaluation of machine translation. In *ACL*, 2002. 13

[49] Aditya Patel, Ashish Kumar Khandual, Kavya Kumar, and Shreya Kumar. Persistence of vision display-a review. *IOSR Journal of Electrical and Electronics Engineering*, 10(4):36–40, 2015. 2

[50] Runqi Qiao, Qiuna Tan, Guanting Dong, Minhui Wu, Chong Sun, Xiaoshuai Song, Zhuoma GongQue, Shanglin Lei, Zhe Wei, Miaoxuan Zhang, Runfeng Qiao, Yifan Zhang, Xiao Zong, Yida Xu, Muxi Diao, Zhimin Bao, Chen Li, and Honggang Zhang. We-math: Does your large multimodal model achieve human-like mathematical reasoning?, 2024. 2

[51] Runqi Qiao, Qiuna Tan, Minghan Yang, Guanting Dong, Peiqing Yang, Shiqiang Lang, Enhui Wan, Xiaowan Wang, Yida Xu, Lan Yang, Chong Sun, Chen Li, Jing Lyu, and Honggang Zhang. V-thinker: Interactive thinking with images, 2025.

[52] Runqi Qiao, Qiuna Tan, Peiqing Yang, Yanzi Wang, Xiaowan Wang, Enhui Wan, Sitong Zhou, Guanting Dong, Yuchen Zeng, Yida Xu, Jie Wang, Chong Sun, Chen Li, and Honggang Zhang. We-math 2.0: A versatile mathbook system for incentivizing visual mathematical reasoning, 2025. 2

[53] Guijie Quan, Wenguan Wang, Zhibo Tian, Fan Ma, and Yi Yang. Psychometry: An omnifit model for image reconstruction from human brain activity. In *CVPR*, 2024. 2

[54] Eve Rabinoff. Human perception. In *Human Perception*, pages 43–70. Northwestern University Press, 2018. 2

[55] Aditya Ramesh, Prafulla Dhariwal, Alex Nichol, Casey Chu, and Mark Chen. Hierarchical text-conditional image generation with clip latents. *arXiv preprint arXiv:2204.06125*, 2022. 3

[56] Rita Ramos, Bruno Martins, Desmond Elliott, and Yova Kementchedjhieva. Smallcap: Lightweight image captioning prompted with retrieval augmentation. In *CVPR*, 2023. 2

[57] Hanoona Rasheed, Muhammad Uzair Khattak, Muhammad Maaz, Salman Khan, and Fahad Shahbaz Khan. Fine-tuned clip models are efficient video learners. In *CVPR*, 2023. 6, 15

[58] Robin Rombach, Andreas Blattmann, Dominik Lorenz, Patrick Esser, and Björn Ommer. High-resolution image synthesis with latent diffusion models. In *CVPR*, 2022. 3

[59] Olaf Ronneberger, Philipp Fischer, and Thomas Brox. U-net: Convolutional networks for biomedical image segmentation, 2015. 17

[60] Simon Scholler, Sebastian Bosse, Matthias Sebastian Treder, Benjamin Blankertz, Gabriel Curio, Klaus-Robert Muller, and Thomas Wiegand. Toward a direct measure of video quality perception using eeg. *IEEE Transactions on Image Processing*, 21(5):2619–2629, 2012. 2

[61] Paul Scotti, Atmadeep Banerjee, Jimmie Goode, Stepan Shabalin, Alex Nguyen, Aidan Dempster, Nathalie Verlinde, Elad Yundler, David Weisberg, Kenneth Norman, et al. Reconstructing the mind's eye: fmri-to-image with contrastive learning and diffusion priors. In *NeurIPS*, 2024. 2

[62] Paul Steven Scotti, Mihir Tripathy, Cesar Torrico, Reese Kneeland, Tong Chen, Ashutosh Narang, Charan Santhirasegaran, Jonathan Xu, Thomas Naselaris, Kenneth A Norman, et al. Mindeye2: Shared-subject models enable fmri-to-image with 1 hour of data. In *ICML*, 2024. 2

[63] Uriel Singer, Adam Polyak, Thomas Hayes, Xi Yin, Jie An, Songyang Zhang, Qiyuan Hu, Harry Yang, Oron Ashual, Oran Gafni, and et al. Make-a-video: Text-to-video generation without text-video data. *arXiv preprint arXiv:2209.14792*, 2022. 3

[64] Leslie N. Smith and Nicholay Topin. Super-convergence: Very fast training of neural networks using large learning rates. *arXiv preprint arXiv:1708.07120*, 2018. 17

[65] Jingyuan Sun, Mingxiao Li, Zijiao Chen, and Marie-Francine Moens. Neurocine: Decoding vivid video sequences from human brain activties. *arXiv preprint arXiv:2402.01590*, 2024. 2, 3

[66] Michael J. Swain and Dana H. Ballard. Color indexing. *International Journal of Computer Vision*, 7(1):11–32, 1991. 6

[67] Yu Takagi and Shinji Nishimoto. High-resolution image reconstruction with latent diffusion models from human brain activity. In *CVPR*, 2023. 2

[68] Qiuna Tan, Runqi Qiao, Guanting Dong, YiFan Zhang, Minhui Wu, Jiapeng Wang, Miaoxuan Zhang, Yida Xu, Chong Sun, Chen Li, and Honggang Zhang. Ocr-critic: Aligning multimodal large language models' perception through critical feedback. In *ACMMM*, 2025. 2

[69] Zhan Tong, Yibing Song, Jue Wang, and Limin Wang. Videomae: Masked autoencoders are data-efficient learners for self-supervised video pre-training. In *NeurIPS*, 2022. 6, 15

[70] Leslie G Ungerleider, Susan M Courtney, and James V Haxby. A neural system for human visual working memory. *Proceedings of the National Academy of Sciences*, 95 (3):883–890, 1998. 2

[71] C. Wang, H. Yan, W. Huang, J. Li, Y. Wang, Y. S. Fan, W. Sheng, T. Liu, R. Li, and H. Chen. Reconstructing rapid natural vision with fmri-conditional video generative adversarial network. *Cerebral Cortex*, 32(20):4502–4511, 2022. 3, 6

[72] Haonan Wang, Qixiang Zhang, Lehan Wang, Xuanqi Huang, and Xiaomeng Li. Neurons: Emulating the human visual cortex improves fidelity and interpretability in fmri-to-video reconstruction. In *ICCV*, 2025. 6, 7

[73] Jianfeng Wang, Zhengyuan Yang, Xiaowei Hu, Linjie Li, Kevin Lin, Zhe Gan, Zicheng Liu, Ce Liu, and Lijuan Wang. Git: A generative image-to-text transformer for vision and language. *arXiv preprint arXiv:2205.14100*, 2022. 2

[74] Shizun Wang, Songhua Liu, Zhenxiong Tan, and Xinchao Wang. Mindbridge: A cross-subject brain decoding framework. In *CVPR*, 2024. 2

[75] Zicheng Wang, Zhen Zhao, Luping Zhou, and Parashkev Nachev. Unibrain: A unified model for cross-subject brain decoding. *arXiv preprint arXiv:2412.19487*, 2024. 2

[76] Haiguang Wen, Junxing Shi, Yizhen Zhang, Kun-Han Lu, Jiayue Cao, and Zhongming Liu. Neural encoding and decoding with deep learning for dynamic natural vision. *Cerebral Cortex*, 28(12):4136–4160, 2017. 2, 3, 5, 6, 17

[77] Jay Zhangjie Wu, Yixiao Ge, Xintao Wang, Stan Weixian Lei, Yuchao Gu, Yufei Shi, Wynne Hsu, Ying Shan, Xiaohu Qie, and Mike Zheng Shou. Tune-a-video: One-shot tuning of image diffusion models for text-to-video generation. In *ICCV*, 2023. 7, 16

[78] Weihao Xia, Raoul de Charette, Cengiz Oztireli, and Jing-Hao Xue. Dream: Visual decoding from reversing human visual system. In *WACV*, 2024. 2

[79] Weihao Xia, Raoul de Charette, Cengiz Oztireli, and Jing-Hao Xue. Umbrae: Unified multimodal brain decoding. In *ECCV*, 2024. 2

[80] Le Xue, Manli Shu, Anas Awadalla, Jun Wang, An Yan, Senthil Purushwalkam, Honglu Zhou, Viraj Prabhu, Yutong Dai, Michael S Ryoo, Shrikant Kendre, Jieyu Zhang, Can Qin, Shu Zhang, Chia-Chih Chen, Ning Yu, Juntao Tan, Tulika Manoj Awalgaonkar, Shelby Heinecke, Huan Wang, Yejin Choi, Ludwig Schmidt, Zeyuan Chen, Silvio Savarese, Juan Carlos Niebles, Caiming Xiong, and Ran Xu. xgen-mm (blip-3): A family of open large multimodal models. *arXiv preprint arXiv:2408.08872*, 2024. 2, 13

[81] Lan Yang, Minghan Yang, Ke Li, Honggang Zhang, Kaiyue Pang, and Yi-Zhe Song. Synmind: Reducing semantic hallucination in fmri-based image reconstruction. *arXiv preprint arXiv:2601.17857*, 2026. 2

[82] Elahe Yargholi and Gholam-Ali Hossein-Zadeh. Brain decoding-classification of hand written digits from fmri data employing bayesian networks. *Frontiers in Human Neuroscience*, 10, 2016. 2

[83] Semir Zeki and Stewart Shipp. The functional logic of cortical connections. *Nature*, 335(6188):311–317, 1988. 8

[84] Boqiang Zhang, Kehan Li, Zesen Cheng, Zhiqiang Hu, Yuqian Yuan, Guanzheng Chen, Sicong Leng, Yuming Jiang,

Hang Zhang, Xin Li, Peng Jin, Wenqi Zhang, Fan Wang, Lidong Bing, and Deli Zhao. Videollama 3: Frontier multimodal foundation models for image and video understanding. *arXiv preprint arXiv:2501.13106*, 2025. 3

[85] Hang Zhang, Xin Li, and Lidong Bing. Video-llama: An instruction-tuned audio-visual language model for video understanding. *arXiv preprint arXiv:2306.02858*, 2023. 13

[86] Yuanhan Zhang, Jinming Wu, Wei Li, Bo Li, Zejun Ma, Ziwei Liu, and Chunyuan Li. Video instruction tuning with synthetic data. *arXiv preprint arXiv:2410.02713*, 2024. 3

[87] Yuanhan Zhang, Jinming Wu, Wei Li, Bo Li, Zejun Ma, Ziwei Liu, and Chunyuan Li. Llava-video: Video instruction tuning with synthetic data. *arXiv preprint arXiv:2410.02713*, 2025. 13

[88] Denny Zhou, Nathanael Schärli, Le Hou, Jason Wei, Nathan Scales, Xuezhi Wang, Dale Schuurmans, Claire Cui, Olivier Bousquet, Quoc V Le, and Ed H. Chi. Least-to-most prompting enables complex reasoning in large language models. In *ICLR*, 2023. 3, 13

[89] Lin Zhu, Siwei Dong, Jianing Li, Tiejun Huang, and Yonghong Tian. Ultra-high temporal resolution visual reconstruction from a fovea-like spike camera via spiking neuron model. *IEEE Transactions on Pattern Analysis and Machine Intelligence*, 45(1):1233–1249, 2022. 2

A. SemMiner

A.1. The Implementation Details

Since the objective of *SemMiner* is to utilize a Multimodal Large Language Model (MLLM) to generate multi-level semantic descriptions of a video from diverse perspectives, directly prompting the MLLM for this complex task often results in hallucinations or inaccurate content. To address this, we decompose the overall objective into a sequence of ordered subtasks—forming a prompt chain—that guides the MLLM progressively from simpler prompts to more complex ones. This step-by-step prompting strategy enhances the model's reasoning ability and output accuracy, while significantly reducing the risk of generating false or unreliable information [28, 32, 40, 88].

SemMiner adopts a two-stage pipeline prompting strategy. In Stage 1, a basic prompt P_{basic} is used to produce a concise core event summary C_{basic}, which serves as an anchoring "rein" to constrain and guide subsequent generation. Without this focused summary, the following caption generation process is prone to semantic drift. In Stage 2, *SemMiner* uses three specialized prompts in conjunction with C_{basic} to generate three decoupled semantic descriptions: a static anchor description (C_{anchor}) of the initial frame, a motion-focused narrative (C_{motion}) describing the dynamic content, and a holistic summary (C_{holi}) that integrates both static and dynamic elements into a coherent spatio-temporal account. The specific prompt templates used in our experiments are illustrated in Figure.7.

A.2. The Results of SemPrompt

In this section, we randomly sample a video from the CC2017 dataset to qualitatively evaluate the descriptions generated by *SemMiner*. As shown in Figure.7 and Figure.8, we first present the semantic caption produced by BLIP2[80], a widely-used video description model in prior fMRI-based video reconstruction works[15, 43]. It is evident that BLIP2 generates a coarse, static scene description and fails to capture the temporal dynamics of the video. In contrast, the multi-level descriptions generated by *SemMiner* —namely C_{anchor}, C_{motion}, and C_{holi}—are significantly more fine-grained and informative. The C_{anchor} description accurately captures the visual content of the initial frame, identifying not only salient objects and scene types (*e.g.*, "a young woman standing in a wheat field") but also detailing spatial layout and appearance features (*e.g.*, "wearing a short-sleeved blouse of a distinct mustard-yellow color and gently cradling a small bundle of golden-brown wheat stalks in her hands"). Similarly, C_{motion} and C_{holi} provide coherent and semantically rich accounts of the dynamic processes and holistic scene context, respectively, demonstrating the effectiveness of *SemMiner* in capturing multi-faceted video semantics.

Additionally, we quantitatively compare the average number of tokens in the descriptions generated by BLIP2 and *SemMiner*, as shown in Table 4. It is evident that BLIP2 produces relatively short captions, with an average of only 10.6 tokens. In contrast, *SemMiner* generates significantly richer descriptions, with averages of 32.8, 41.1, and 52.8 tokens for C_{anchor}, C_{motion}, and C_{holi}, respectively. These results highlight the ability of *SemMiner* to provide more detailed and semantically informative supervision signals, which in turn facilitate higher-quality neural decoding and video reconstruction.

caption type	BLIP2	C_{anchor}	C_{motion}	C_{holi}
number	10.6	32.8	41.1	52.8

Table 4. Average number of tokens in the descriptions generated by BLIP2 and *SemMiner* on CC2017 Datasets.

A.3. Caption Similarity Analysis

To quantitatively assess the semantic gap between the captions generated by *SemMiner*, and to verify that each description indeed captures a distinct perspective of the video stimulus, we evaluate the semantic similarity among them using a set of standard language similarity metrics [22, 48]. As shown in Table 5, the results reveal clear semantic divergence across the generated descriptions (C_{anchor}, C_{motion}, and C_{holi}), confirming that *SemMiner* effectively extracts complementary and perspective-specific semantic information from the input video.

Pair	BLEU-1	BLEU-4	METEOR	ROUGE-1	ROUGE-L	CLIP-S
C_{anchor} v.s. C_{motion}	0.171	0.022	0.186	0.275	0.207	0.655
C_{anchor} v.s. C_{holi}	0.197	0.028	0.222	0.304	0.225	0.665
C_{motion} v.s. C_{holi}	0.270	0.067	0.292	0.400	0.293	0.744

Table 5. Semantic Similarity Experiments of different caption pairs. Lower values across all metrics indicate greater semantic dissimilarity.

A.4. The Impact of Different VLLM

To evaluate the generalizability of *SemMiner*, we integrate three different vision-language large models (VLLMs)—Video-LLaMA [85], Qwen2.5-VL [2], and LLaVA-Video [87]—to generate semantic targets, using the same implementation details described in Appendix A.1.

The comparison results, presented in Table 6, show that while the optimal performance on individual metrics varies slightly across different VLLMs, all configurations achieve consistently strong and competitive reconstruction quality. The consistently high results confirm that the effectiveness of *SemMiner* does not rely on any specific VLLM. This robustness is rooted in its core design — a hierarchical seman-

Seen Video:

BLIP2 Generated Output: a girl in a yellow shirt is standing in a field of wheat.

SemMiner - Stage 1

P_{basic} : Please provide a concise summary of the core events in this video. Your description must be strictly under20 words.

C_{basic} : A young woman in a wheat field, holding stalks of wheat, looks up to face the camera.

SemMiner - Stage 2

P_{anchor}:

Conditioned on the provided summary, $\{C_{basic}\}$, generate a detailed textual description of the video's initial frame. The description must detail key objects, their attributes (e.g., color, shape), and the overall scene setting. The generated text should answer the implicit question: 'What visual semantics would a human observer perceive from this stimulus?' The final output must be clear and precise, suitable for use as an input to a text-to-image model.

C_{anchor}:

The initial frame presents a photorealistic, sun-drenched medium close-up of a young woman standing in a wheat field. The central figure has long, straight, dark brown hair; her head is slightly tilted down with her eyes closed. She is wearing a short-sleeved blouse of a distinct mustard-yellow color and gently cradles a small bundle of golden-brown wheat stalks in her hands. The setting is an outdoor field where the background is softly out of focus, showing a mix of green and golden foliage under bright, natural sunlight.

P_{motion}:

Conditioned on the provided summary, $\{C_{basic}\}$, generate a description centered on the motion and dynamic actions of the principal objects in the video. This description should detail attributes such as movement direction, speed, posture changes, and interaction timing. The final output must be a detailed narrative, strictly constrained to a maximum length of 50 tokens.

C_{motion}:

The woman's head, initially tilted down with eyes closed, lifts in a slow and smooth motion. As her head rises, her eyes open, and her gaze deliberately shifts upward from a downward glance to look directly forward into the camera. This single, graceful action concludes with direct eye contact at the end of the clip.

P_{holi}:

Conditioned on the preceding summary, $\{C_{basic}\}$, generate a holistic description of the full video scene. This description must integrate the static background with the dynamic actions of the primary objects, detailing how they move through space and interact with the environment. The output should be a detailed narrative of approximately 60 words, presented without any introductory or concluding remarks.

C_{holi}:

In a sun-drenched wheat field, a young woman is captured in a medium close-up against a soft-focus golden and green background. Initially still and contemplative, her head is tilted down with her eyes closed as she cradles a bundle of wheat stalks. A slow, deliberate motion begins as she gracefully lifts her head. Her eyes open simultaneously with this fluid movement, her gaze traveling upward from the wheat to meet the camera lens directly, establishing a clear line of engagement.

Figure 7. Prompt templates used in *SemMiner* and qualitative comparison of captions generated by BLIP2 and *SemMiner*. *SemMiner* employs four distinct prompt templates to generate hierarchical semantic descriptions for a given video stimulus. The process begins with the Basic Prompt P_{basic}, which establishes a core semantic summary to anchor subsequent generations. This is followed by three specialized prompts in stage 2: (i) P_{anchor}, which produces a detailed description of the initial frame, optimized for guiding text-to-image models; (ii) P_{motion}, which focuses on extracting dynamic information such as object motion, direction, speed, and posture changes; and (iii) P_{holi}, which integrates static and dynamic elements to form a coherent, high-level narrative of the entire video. Compared to BLIP2, which tends to generate short and static descriptions, *SemMiner* provides richer and more perspective-specific captions.

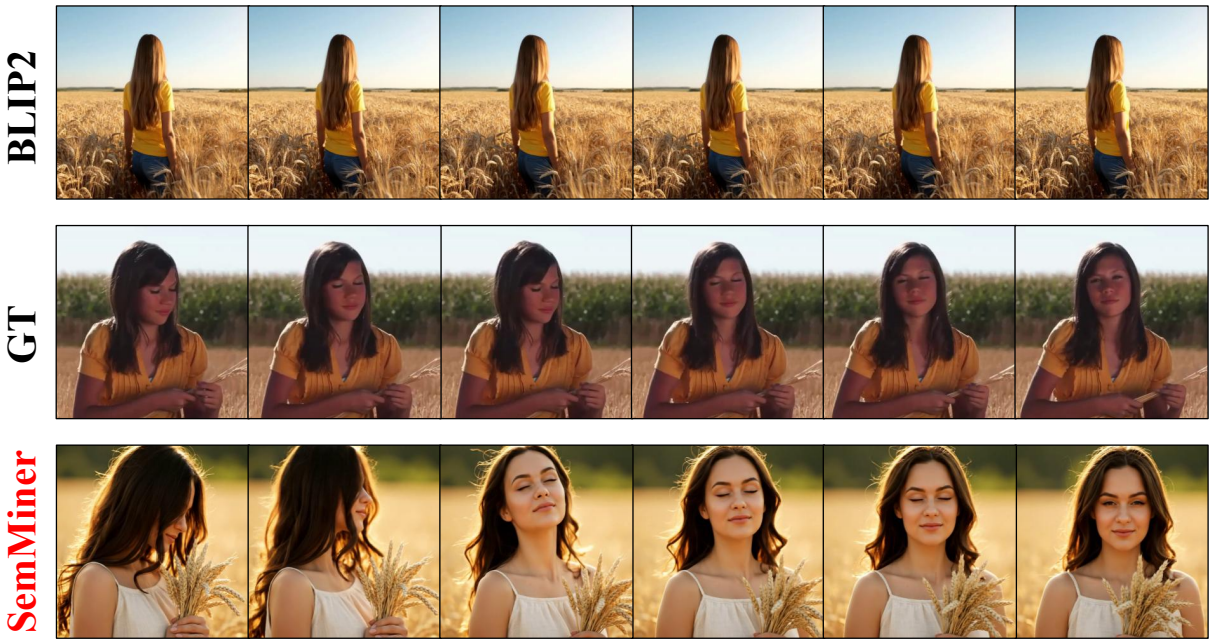

Figure 8. Video generated from BLIP2 caption(upper) and SemMiner(lower). The middle is the target video.

tic prompting strategy that reliably guides diverse VLLMs to generate rich, structured, and multi-perspective video descriptions, thereby providing high-quality semantic supervision for fMRI-based video reconstruction.

B. Evaluation Metrics

We devised a multi-level evaluation protocol to comprehensively assess the performance of our video reconstruction model. This protocol systematically quantifies the fidelity of reconstructed videos to the original visual stimuli across three key dimensions: semantic, pixel, and spatiotemporal.

B.1. Semantic-level

Semantic-level metrics quantitatively assess the conceptual alignment between the reconstructed and original videos. We employ two methods for this purpose: the N-way Top-1 accuracy test and the VIFI-Score. **N-way Top-1 Accuracy** measures the precision of semantic content reconstruction using a dual strategy: (1) Dynamic Content. To evaluate the semantic fidelity of dynamic events, a VideoMAE [69] model pretrained on the Kinetics-400 dataset classifies both the original and reconstructed videos, after which the consistency of their predicted class labels is compared. (2) Static Content. To assess the accuracy of static elements, a ViT-For-Image-Classification model [11] pretrained on ImageNet performs frame-by-frame classification.

VIFI-Score:This metric is calculated using a VIFI-CLIP [57] model that has been fine-tuned on video datasets. The model extracts high-level feature embeddings from both the original and reconstructed videos. The final VIFI-Score is the cosine similarity between these two embedding vectors, where a higher value indicates greater semantic congruence.

B.2. Pixel-level

Pixel-level metrics quantitatively assess low-level visual fidelity by directly comparing the reconstructed video to the original visual stimulus. These metrics provide a foundational measure of reconstruction quality by focusing on the accuracy of pixel values and the preservation of fundamental image characteristics.

Peak Signal-to-Noise Ratio (PSNR): A widely adopted metric for quantifying reconstruction error, PSNR is derived from the Mean Squared Error (MSE) between the pixel values of the original and reconstructed images and measures distortion on a logarithmic scale.

Structural Similarity Index (SSIM): This metric evaluates the preservation of structural information between frames. Unlike purely pixel-wise error metrics, SSIM is designed to model perceptual similarity by jointly considering luminance, contrast, and structure.

Hue Similarity: This metric specifically assesses color reproduction accuracy by computing the cosine similarity between the hue channel vectors of the original and reconstructed frames. The hue component is isolated because it represents pure color, independent of saturation and brightness. A high score therefore indicates that the model has successfully reproduced the chromatic ambiance of the original scene, a critical factor for the overall visual experi-

MLLM	Semantic-Level					Pixel-Level			ST-Level	
	2-way-I↑	2-way-V↑	50-way-I↑	50-way-V↑	VIFI-score↑	SSIM↑	PSNR↑	Hue-pcc↑	CLIP ↑	EPE ↓
VideoLlama	**0.826**	0.860	**0.211**	0.239	0.590	**0.330**	**9.626**	0.841	**0.502**	4.768
Qwen2.5-vl	0.821	**0.863**	0.203	**0.242**	0.589	0.299	9.03	0.858	0.496	**4.40**
Llava-Video	0.815	0.855	0.207	0.228	**0.591**	0.309	8.96	**0.861**	0.493	4.65

Table 6. Ablation study on the CC2017 dataset investigating performance variations when using different VLLMs within the *SemMiner* framework.

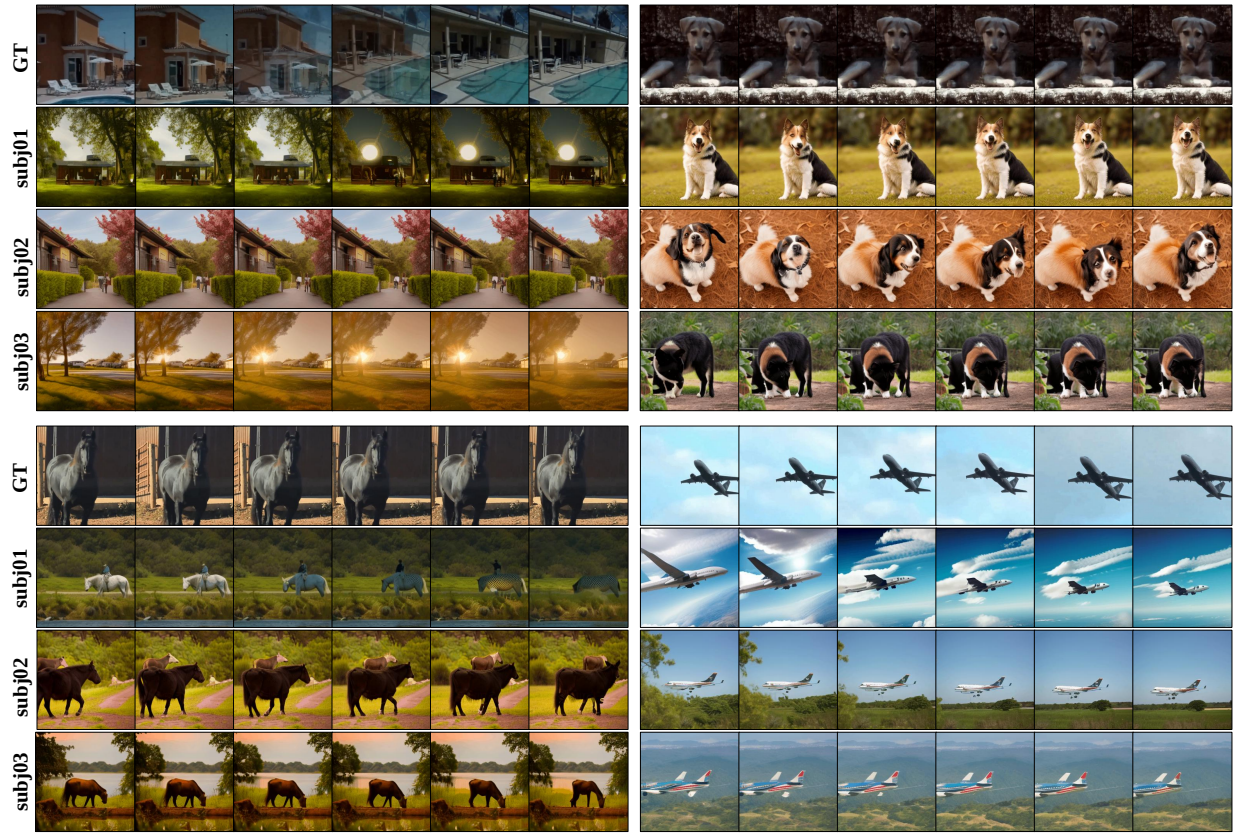

Figure 9. More reconstruction results on the CC2017 dataset from three subjects.

ence.

B.3. Spatiotemporal (ST)-level

Spatiotemporal (ST) metrics are designed to evaluate the dynamic aspects of a reconstructed video, focusing on its temporal coherence and motion representation accuracy. These metrics are crucial for assessing a model's ability to generate realistic and continuous sequences of events.

CLIP-pcc [77]: This metric assesses the temporal smoothness and semantic continuity of a video sequence. It is calculated by using a CLIP (ViT-B/32) model to extract feature embeddings for each frame and then averaging the cosine similarity across all adjacent frame pairs.

Endpoint Error (EPE [3]): This metric provides a precise quantification of motion reconstruction fidelity. It is defined as the mean Euclidean distance between the optical flow vectors of the reconstructed and original videos. By directly comparing these predicted motion fields, EPE serves as a critical indicator of the model's capability to accurately reproduce the trajectories and velocities of objects within the scene.

C. Implementation Details

C.1. Hyperparameter Settings

For the Semantic Alignment Decoder, we utilized the AdamW [41] optimizer. The training was conducted for 100 epochs with a batch size of 96. A cosine annealing schedule was employed to manage the learning rate, with a maximum value set to 1e-4. λ_{refine} and $\lambda_{\text{SoftCLIP}}$ are set to

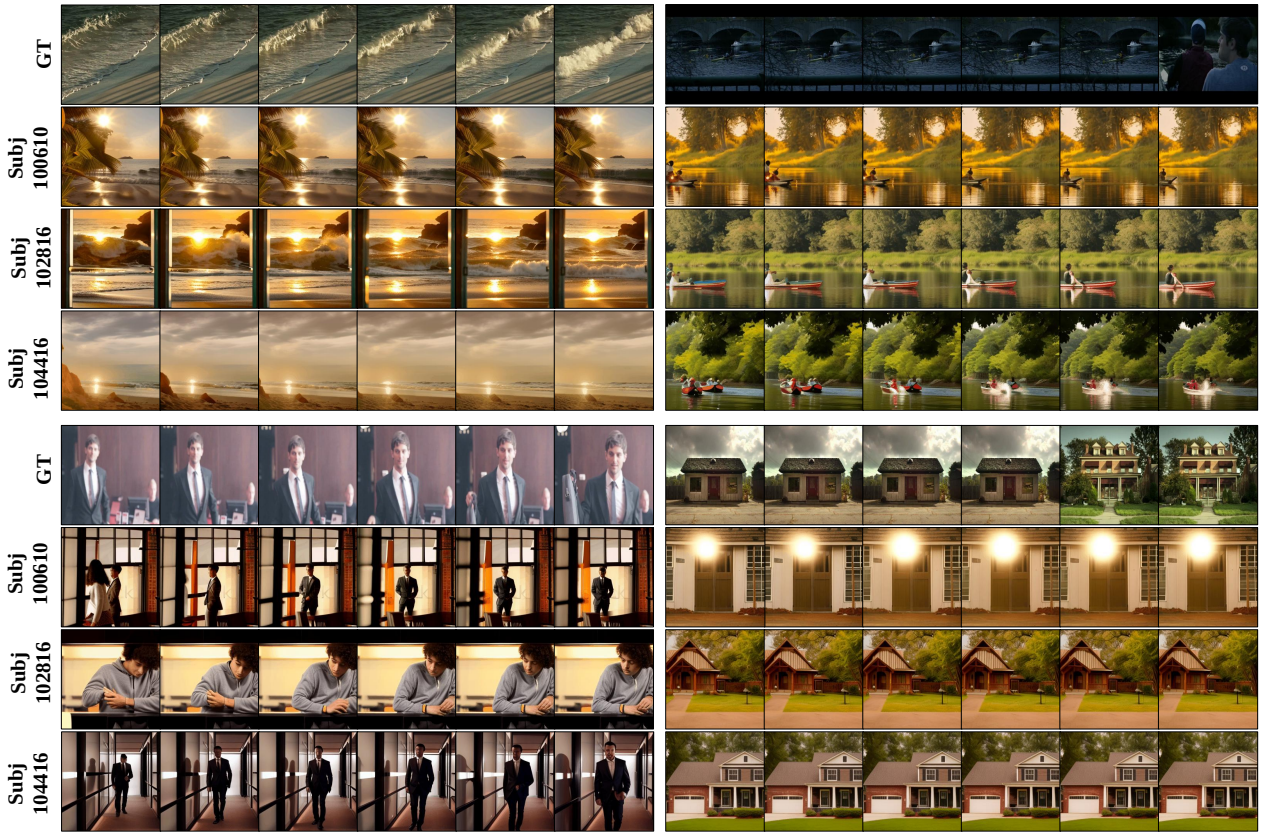

Figure 10. More reconstruction results on the HCP dataset from three subjects.

0.5 and 0.1, respectively. Furthermore, to mitigate the risk of overfitting arising from the scarcity of fMRI-video data pairs, we incorporated the Mixco data augmentation technique.

$$x_{mix_{i,j}} = \alpha x'_i + (1-\alpha)x'_j, \tag{14}$$

where $\alpha \sim \text{Beta}(0.15, 0.15)$ is a mixing coefficient sampled from the Beta distribution, and x'_i is the i-th latent representation to the x'-encoded batch.

For the Motion Adaptation Decoder, the AdamW optimizer was also employed, and the model was trained for 100 epochs with a batch size of 20. The learning rate was governed by a OneCycleLR [64] schedule, with the maximum learning rate configured to 3e-4. Notably, λ_{spat} and λ_{temp}, were not pre-defined hyperparameters. Instead, they were implemented as learnable parameters that are automatically optimized during the training process.

C.1.1. Model Architecture

For Semantic Alignment Decoder, we use a linear layer to implement the subject-specific mapper $f^{\theta_m}_{\text{SAD}}$, which maps voxels $x \in \mathbb{R}^{D_m}$ to the shared space $\mathbb{R}^{4096}$. f^{MLP}_{SAD} is implemented as a four-layer perceptual machine with output channels specified as $\{4096, 4096, 4096, 77 \times 768\}$, using the GELU nonlinear activation function. The (f^{Refine}_{SAD}) module uses a Transformer architecture with 4 layers, each containing 8 attention heads of dimension 64.

For the Motion Adaptation Decoder, f^{proj}_{MAD} is composed of a linear layer and a four-layer Multi-Layer Perceptron with output channels specified as $\{256, 6 \times 4096, 6 \times 4096, 4096, 6 \times (64 * 7 * 7)\}$.The fusion attention module is a lightweight decoder with a UNet-like [59] architecture, consisting of one UNetMidBlock2D and three cascaded AttnUpDecoderBlock2D upsampling blocks. The architecture takes a 64-channel, 7x7 feature map as input and progressively upsamples it to a 4-channel, 28x28 latent representation.

D. More Results

We present further examples of video reconstruction across multiple subjects from both the CC2017 [76] and HCP [44] datasets, as illustrated in Figure.9 and Figure.10.

D.1. Neural Interpretability

To further validate the neural interpretability of the proposed framework, we generated voxel-wise importance

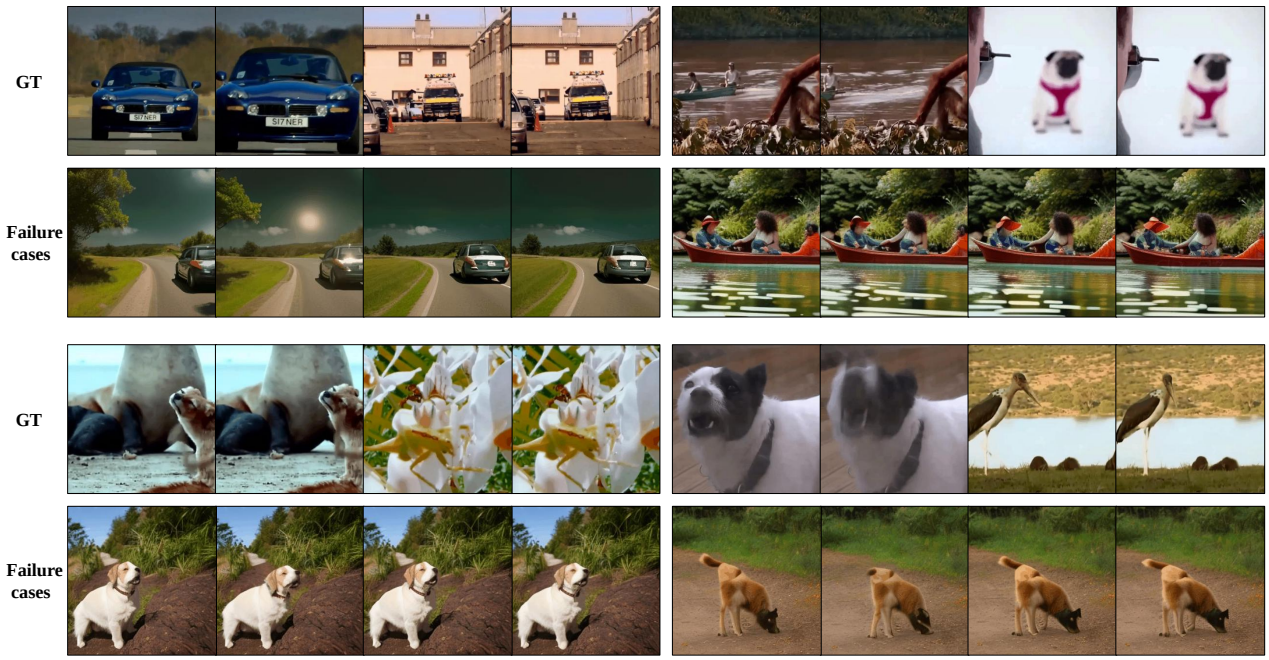

Figure 11. Reconstruction failure cases.

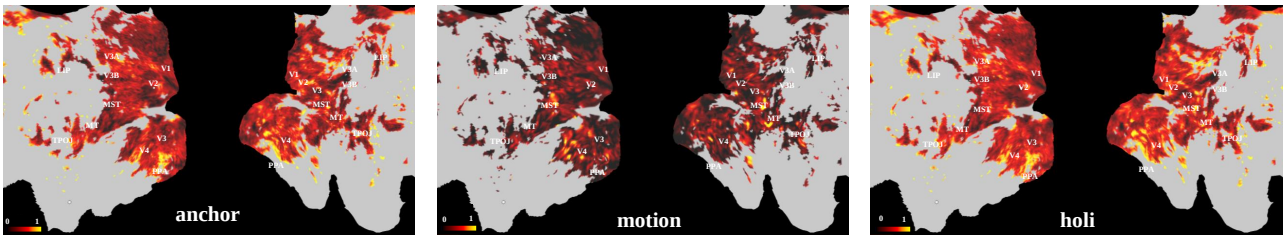

Figure 12. Importance visualization of different ROIs for Subject 2, based on the fitted weights from the first layer of the SFD. Weights from each module are averaged and normalized to the $[0, 1]$ range for comparison.

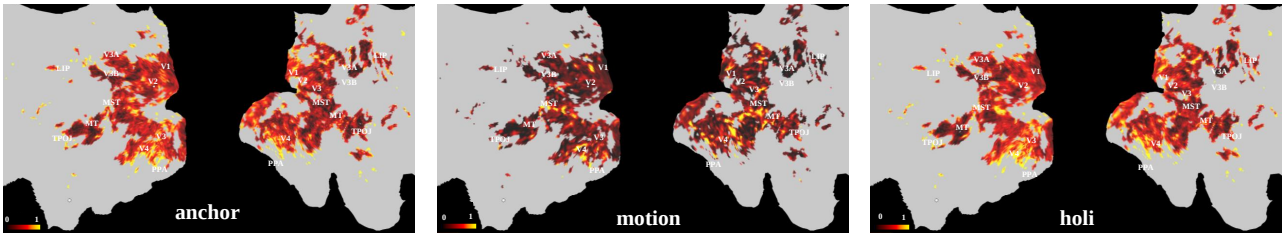

Figure 13. Importance visualization of different ROIs for Subject 3, based on the fitted weights from the first layer of the SFD. Weights from each module are averaged and normalized to the $[0, 1]$ range for comparison.

maps of the cerebral cortex for Subjects 2 and 3 from the CC2017 dataset, as depicted in Figure.12 and Figure.13. The experimental results for these subjects reveal voxel importance distribution patterns that are highly similar to those observed for Subject 1: The anchor component's activations were predominantly concentrated in visual cortical areas. The motion component exhibited stronger activations in brain regions specialized for motion processing. The holistic component displayed a balanced activation pattern across both of these functional regions. This hierarchical semantic mapping enables *SemVideo* to generate more perceptually faithful reconstructions and similar activation distributions across subjects demonstrate stable feature capture for both static semantics and dynamic behaviors.

D.2. Failure cases

To facilitate a comprehensive and objective assessment of $SemVideo$, we analyze several of its reconstruction failure cases in Figure.11. A primary cause of these failures stems from the inherent data acquisition paradigm. Specifically, the experimental data is created by evenly segmenting longer videos, which introduces abrupt content transitions at the boundaries of the resulting clips. Our model, $SemVideo$, struggles to replicate these sudden shifts in the reconstructed outputs.